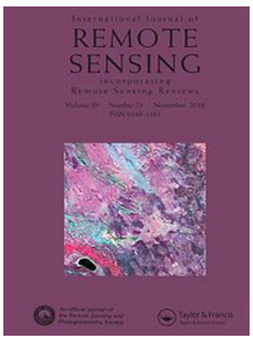

International Journal of Remote Sensing

ISSN: 0143-1161 (Print) 1366-5901 (Online) Journal homepage: http://www.tandfonline.com/loi/tres20

Multiple classifier systems for classification of multifrequency PolSAR images with limited training samples

Iman Khosravi, Abdolreza Safari & Saeid Homayouni

To cite this article: Iman Khosravi, Abdolreza Safari & Saeid Homayouni (2018) Multiple classifier systems for classification of multifrequency PolSAR images with limited training samples, International Journal of Remote Sensing, 39:21, 7547-7567, DOI: 10.1080/01431161.2018.1471543

To link to this article: https://doi.org/10.1080/01431161.2018.1471543

INTERNATIONAL JOURNAL OF REMOTE SENSING
2018, VOL. 39, NO. 21, 7547–7567
https://doi.org/10.1080/01431161.2018.1471543

Taylor & Francis
Taylor & Francis Group

Multiple classifier systems for classification of multifrequency PolSAR images with limited training samples

Iman Khosravi[a], Abdolreza Safari[a] and Saeid Homayouni[b]

[a]School of Surveying and Geospatial Engineering, College of Engineering, University of Tehran, Tehran, Iran; [b]Department of Geography, Environment and Geomatics, University of Ottawa, Ottawa, Canada

ABSTRACT

The aim of this article is to improve land-cover classification accuracy from multifrequency full-polarimetric synthetic aperture radar (PolSAR) observations using multiple classifier systems (MCSs) when limited training samples are available. Two types of popular MCSs, tree-based MCSs and neural-based MCSs, were compared with individual decision tree (DT) and neural network methods. Moreover, an objective majority voting (OMV) was proposed and compared with majority voting (MV) and weighted MV (WMV) to fuse the results of the MCSs. Experimental tests were performed on three benchmark PolSAR data sets with different frequencies (X, C, and L) over the San Francisco Bay, CA. The results indicated (1) tree-based MCSs and neural-based MCSs, in general, produced higher overall, producer's and user's accuracies than the related individual methods, i.e. DT and NN, with limited training samples; (2) tree-based MCSs were also often more accurate and much faster than neural-based MCSs; (3) regarding robustness, among the MCSs, random forest showed higher stability while bagging showed lower stability in the classification of three PolSAR data sets; (4) the OMV proposed in this article usually outperformed its competitors, i.e. MV and WMV; (5) the results obtained by the methods from the C-band data set were more accurate and more reliable than those obtained from the X- and L-band data sets.

ARTICLE HISTORY
Received 23 November 2017
Accepted 20 April 2018

1. Introduction

Synthetic aperture radar (SAR) image has recently become a favourable remotely sensed source for land-cover classification. Unlike optical imaging, SAR observations are almost unaffected by weather and illumination conditions (Gens 2008). Full-polarimetric SAR (PolSAR) sensor is a particular type of SAR sensor that has recently received considerable attention in land-cover mapping and monitoring (Alberga, Satalino, and Staykova 2008; McNairn et al. 2009; Shah Hosseini et al. 2011). Compared with single and dual-polarized SAR data, the advantage of PolSAR data is the potential of extracting a variety of polarimetric features, such as polarization intensities and target decomposition parameters for object detection and classification. These features are, indeed, very promising

CONTACT Iman Khosravi iman.khosravi@ut.ac.ir School of Surveying and Geospatial Engineering, College of Engineering, University of Tehran, Tehran, Iran
Supplemental data for this article can be accessed here.

in the detection of various land covers and can potentially increase classification accuracy (Alberga 2007; Lardeux et al. 2009; Lonnqvist et al. 2010; Du et al. 2014; Salehi, Sahebi, and Maghsoudi 2014). Furthermore, different frequencies of PolSAR imagery such as X-, C-, L-, and P-bands can offer unique and diverse information for land-cover mapping because each frequency band is sensitive to a surface scale (Mehta et al. 2014; Liu et al. 2015). Over the last two decades, some studies have used different frequencies for land-cover classification in agricultural areas (Rosenthal, Blanchard, and Banchrd 1985; Chen et al. 1996; Ferrazzoli et al. 1997; Ferrazzoli, Guerriero, and Schiavon 1999; Inoue et al. 2002; Mehta et al. 2014). However, there is little research that has examined different frequencies for land-cover classification in urban areas.

Regarding classification algorithms for land-cover mapping from SAR and PolSAR observations, various supervised and unsupervised algorithms have already been proposed. Traditional methods such as Bayesian and maximum likelihood were used in some studies (e.g. Van Zyl and Burnette 1992; Alberga 2007; Entezari, Motagh, and Mansouri 2012; Shokrollahi and Ebadi 2016). A specific version of the maximum likelihood for SAR classification, i.e. Wishart maximum likelihood, has been used in many studies (e.g. Lee, Grunes, and Kwok 1994; Lardeux et al. 2009; Lonnqvist et al. 2010; Ma et al. 2014; Salehi, Sahebi, and Maghsoudi 2014; Qi et al. 2015; Shokrollahi and Ebadi 2016). These traditional methods are parametric methods, i.e. they are strongly dependent on the distribution of data. Non-parametric algorithms such as *k*-means, fuzzy *c*-means, decision tree (DT), and neural network (NN) have also been used in the literature (e.g. Hara et al. 1994; Bruzzone et al. 2004; Alberga, Satalino, and Staykova 2008; Mishra, Singh, and Yamaguchi 2011; Ma et al. 2014; McNairn et al. 2014; Salehi, Sahebi, and Maghsoudi 2014; Xu, Li, and Brenning 2014; Qi et al. 2015). Although these algorithms are independent of data distribution, they may still face limitations and complexities in the classification tasks with limited training samples.

Support Vector Machine (SVM) and kernel methods are other non-parametric methods that were also used for SAR/PolSAR data classification (e.g. Waske and Van Der Linden 2008; Lardeux et al. 2009; Shah Hosseini et al. 2011; Maghsoudi, Collins, and Leckie 2012; Du et al. 2014; Ma et al. 2014; Niu and Ban 2014; Salehi, Sahebi, and Maghsoudi 2014; Souissi, Ouarzeddine, and Belhadj-Aissa 2014; Uhlmann and Kiranyaz 2014; Qi et al. 2015; Habibi et al. 2016; Shokrollahi and Ebadi 2016). SVM has shown high efficiency with limited training samples, but it has some drawbacks. It is highly sensitive to its kernel function, as well as its parameters. It may also be inefficient in the classification of data in which there are outliers (Mountrakis, Im, and Ogole 2011).

Multiple classifier systems (MCSs) such as boosting, bagging, and random forest (RF) methods have demonstrated their efficiency in data classification with limited training samples (Polikar 2006). Furthermore, MCSs can divide and conquer big data even with the use of weak or unstable classifiers, such as DT and NN. Moreover, they are also exempt from the challenges of SVM, such as sensitivity to parameters or outliers in data (Breiman 2001). There are a few studies that have reported the efficiency of MCSs for the classification of PolSAR images (e.g. Waske and Van Der Linden 2008; Deschamps et al. 2012; Ma et al. 2014; Uhlmann and Kiranyaz 2014; Xu, Li, and Brenning 2014). In Ma et al. (2014), a soft voting method was proposed to combine some base classifiers. The extension of the majority voting (MV) technique should be proceeded more objectively.

This article is dedicated to MCS methods for the classification of three benchmark PolSAR data sets. These three data sets have different frequencies of X-, C-, and L-bands. The goals of this article are summarized as follows: (1) comparing the efficiency and reliability of boosting, bagging, and RF *versus* individual classifiers DT and NN, with a limited number of training samples; (2) comparing three frequencies for land-cover classification in an urban area; and (3) presenting two extended voting techniques and comparing them with the classical MV technique in terms of efficiency and reliability.

2. Methodology

The proposed methodology is presented in Figure 1. It has three main steps: extracting polarimetric features, classifying PolSAR data using some well-known MCSs, and combining the results of the MCSs using voting techniques.

2.1. *Polarimetric features extraction*

PolSAR data can be expressed in the form of Sinclair scattering matrix [**S**], as the first representation. Multi-look covariance and coherency matrices, derived from the scattering matrix, are the second-order representations and are more suitable for analysing distributed and undistributed targets (Salehi, Sahebi, and Maghsoudi 2014). From these three matrices, a variety of useful polarimetric features can be extracted for the classification and mapping of various land covers. They are defined as follows.

2.1.1. *Polarization intensities*

Linearly polarized backscatter intensities ($\boldsymbol{\sigma}_{HH}$, $\boldsymbol{\sigma}_{HV}$, and $\boldsymbol{\sigma}_{VV}$) are the primary feature vectors of PolSAR data that can offer information about the structure of various land covers (McNairn et al. 2009). Moreover, the ratios between linear polarizations ($\boldsymbol{R}_{HHVV}$, $\boldsymbol{R}_{HVHH}$, and $\boldsymbol{R}_{HVVV}$) and the ratios between linear polarizations and the total backscattering coefficient, i.e. span ($\boldsymbol{R}_{HH}$, $\boldsymbol{R}_{HV}$, and $\boldsymbol{R}_{VV}$), have also shown their use in discriminating various land covers (Rignot et al. 1993; Dubois, Van Zyl, and Engman 1995; Entezari, Motagh, and Mansouri 2012). Furthermore, based on the polarization synthesis theory, circularly polarized backscatter intensities ($\boldsymbol{\sigma}_{RR}$, $\boldsymbol{\sigma}_{RL}$, and $\boldsymbol{\sigma}_{LL}$), the ratios between circular polarizations ($\boldsymbol{R}_{RRLL}$, $\boldsymbol{R}_{RLRR}$, and $\boldsymbol{R}_{RLLL}$) and the ratios between circular polarizations and span ($\boldsymbol{R}_{RR}$, $\boldsymbol{R}_{RL}$, and $\boldsymbol{R}_{LL}$), can be useful feature vectors for land-cover classification. These features are defined as (Entezari, Motagh, and Mansouri 2012).

$$\boldsymbol{\sigma}_{HH} = 10\log_{10}|\boldsymbol{S}_{HH}|^2, \quad \boldsymbol{\sigma}_{HV} = 10\log_{10}|\boldsymbol{S}_{HV}|^2, \quad \boldsymbol{\sigma}_{VV} = 10\log_{10}|\boldsymbol{S}_{VV}|^2 \tag{1}$$

$$\begin{aligned} &\boldsymbol{R}_{HHVV} = 10\log_{10}\left(|\boldsymbol{S}_{HH}|^2/|\boldsymbol{S}_{VV}|^2\right), \ \boldsymbol{R}_{HVHH} = 10\log_{10}\left(|\boldsymbol{S}_{HV}|^2/|\boldsymbol{S}_{HH}|^2\right), \\ &\boldsymbol{R}_{HVVV} = 10\log_{10}\left(|\boldsymbol{S}_{HV}|^2/|\boldsymbol{S}_{VV}|^2\right) \end{aligned} \tag{2}$$

$$\begin{aligned} &\boldsymbol{R}_{HH} = 10\log_{10}\left(|\boldsymbol{S}_{HH}|^2/\text{span}\right), \ \boldsymbol{R}_{HV} = 10\log_{10}\left(|\boldsymbol{S}_{HV}|^2/\text{span}\right), \\ &\boldsymbol{R}_{VV} = 10\log_{10}\left(|\boldsymbol{S}_{VV}|^2/\text{span}\right) \end{aligned} \tag{3}$$

where $\boldsymbol{S}_{ij}$ (i, j = {H, V, R, L}) refers to elements of scattering matrix and the subscripts 'H' and 'V' denote the horizontal and vertical linear polarization bases and 'R' and 'L' denote

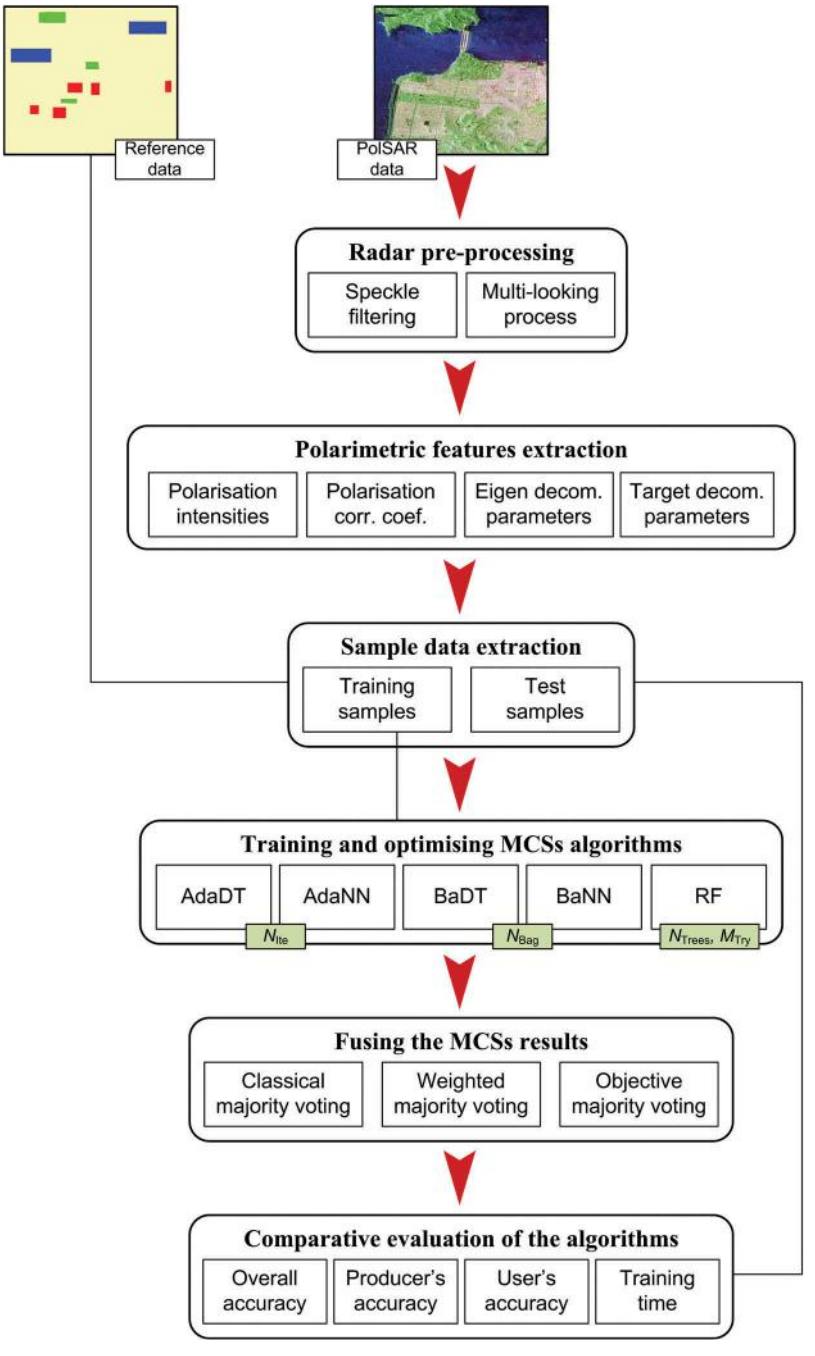

Figure 1. The framework of the proposed methodology.

the right-hand and left-hand circular polarization bases. Moreover, span is defined as follows (Lee and Pottier 2009).

$$\text{span} = |\boldsymbol{S}_{HH}|^2 + 2|\boldsymbol{S}_{HV}|^2 + |\boldsymbol{S}_{VV}|^2 = |\boldsymbol{S}_{RR}|^2 + 2|\boldsymbol{S}_{RL}|^2 + |\boldsymbol{S}_{LL}|^2 \quad (4)$$

2.1.2. *Polarization correlation coefficients*

In addition to polarization intensities, correlation coefficients between a pair of polarizations may be very helpful because correlation coefficient values differ depending on land-cover types (Huang et al. 2017). For example, they have proved to be very promising in distinguishing between man-made and natural covers (Entezari, Motagh, and Mansouri 2012). For PolSAR imagery, three linear polarization correlation vectors ($\boldsymbol{\rho}_{\mathrm{HHVV}}$, $\boldsymbol{\rho}_{\mathrm{HVHH}}$, and $\boldsymbol{\rho}_{\mathrm{HVVV}}$) and three circular polarization correlation vectors ($\boldsymbol{\rho}_{\mathrm{RRLL}}$, $\boldsymbol{\rho}_{\mathrm{RLRR}}$, and $\boldsymbol{\rho}_{\mathrm{RLLL}}$) can be considered. They are defined as (Entezari, Motagh, and Mansouri 2012).

$$\begin{aligned}\boldsymbol{\rho}_{\mathrm{HHVV}} &= \left|\langle \boldsymbol{S}_{\mathrm{HH}}, \boldsymbol{S}_{\mathrm{VV}}^{*}\rangle / \sqrt{\langle \boldsymbol{S}_{\mathrm{HH}}, \boldsymbol{S}_{\mathrm{HH}}^{*}\rangle \langle \boldsymbol{S}_{\mathrm{VV}}, \boldsymbol{S}_{\mathrm{VV}}^{*}\rangle}\right| \\ \boldsymbol{\rho}_{\mathrm{HVHH}} &= \left|\langle \boldsymbol{S}_{\mathrm{HV}}, \boldsymbol{S}_{\mathrm{HH}}^{*}\rangle / \sqrt{\langle \boldsymbol{S}_{\mathrm{HV}}, \boldsymbol{S}_{\mathrm{HV}}^{*}\rangle \langle \boldsymbol{S}_{\mathrm{HH}}, \boldsymbol{S}_{\mathrm{HH}}^{*}\rangle}\right| \\ \boldsymbol{\rho}_{\mathrm{HVVV}} &= \left|\langle \boldsymbol{S}_{\mathrm{HV}}, \boldsymbol{S}_{\mathrm{VV}}^{*}\rangle / \sqrt{\langle \boldsymbol{S}_{\mathrm{HV}}, \boldsymbol{S}_{\mathrm{HV}}^{*}\rangle \langle \boldsymbol{S}_{\mathrm{VV}}, \boldsymbol{S}_{\mathrm{VV}}^{*}\rangle}\right|\end{aligned} \tag{5}$$

$$\begin{aligned}\boldsymbol{\rho}_{\mathrm{RRLL}} &= \left|\langle \boldsymbol{S}_{\mathrm{RR}}, \boldsymbol{S}_{\mathrm{LL}}^{*}\rangle / \sqrt{\langle \boldsymbol{S}_{\mathrm{RR}}, \boldsymbol{S}_{\mathrm{RR}}^{*}\rangle \langle \boldsymbol{S}_{\mathrm{LL}}, \boldsymbol{S}_{\mathrm{LL}}^{*}\rangle}\right| \\ \boldsymbol{\rho}_{\mathrm{RLRR}} &= \left|\langle \boldsymbol{S}_{\mathrm{RL}}, \boldsymbol{S}_{\mathrm{RR}}^{*}\rangle / \sqrt{\langle \boldsymbol{S}_{\mathrm{RL}}, \boldsymbol{S}_{\mathrm{RL}}^{*}\rangle \langle \boldsymbol{S}_{\mathrm{RR}}, \boldsymbol{S}_{\mathrm{RR}}^{*}\rangle}\right| \\ \boldsymbol{\rho}_{\mathrm{RLLL}} &= \left|\langle \boldsymbol{S}_{\mathrm{RL}}, \boldsymbol{S}_{\mathrm{LL}}^{*}\rangle / \sqrt{\langle \boldsymbol{S}_{\mathrm{RL}}, \boldsymbol{S}_{\mathrm{RL}}^{*}\rangle \langle \boldsymbol{S}_{\mathrm{LL}}, \boldsymbol{S}_{\mathrm{LL}}^{*}\rangle}\right|\end{aligned} \tag{6}$$

where <> indicates dot product and * stands for the complex conjugate.

2.1.3. *Target decomposition parameters*

Target decomposition methods can describe the physics of scattering mechanisms of land covers, i.e. surface scattering, double-bounce, and volume scattering (McNairn et al. 2009). They are divided into two coherent and incoherent methods. The coherent methods aim to express the scattering matrix measured by a SAR sensor as a combination of scattering responses of simpler objects or single targets. Pauli decomposition parameter vectors ($|\boldsymbol{\alpha}|^2$, $|\boldsymbol{\beta}|^2$, and $|\boldsymbol{\gamma}|^2$) and Krogager decomposition parameter vectors ($|\boldsymbol{k}_{\mathrm{s}}|^2$, $|\boldsymbol{k}_{\mathrm{d}}|^2$, and $|\boldsymbol{k}_{\mathrm{h}}|^2$) are examples of coherent decomposition. They are defined as (Krogager 1990; Cloude and Pottier 1996).

$$|\boldsymbol{\alpha}|^2 = \left|(\boldsymbol{S}_{\mathrm{HH}} + \boldsymbol{S}_{\mathrm{VV}})/\sqrt{2}\right|^2, \quad |\boldsymbol{\beta}|^2 = \left|(\boldsymbol{S}_{\mathrm{HH}} - \boldsymbol{S}_{\mathrm{VV}})/\sqrt{2}\right|^2, \quad |\boldsymbol{\gamma}|^2 = 2|\boldsymbol{S}_{\mathrm{HV}}|^2 \tag{7}$$

$$\boldsymbol{k}_{\mathrm{s}} = |\boldsymbol{S}_{\mathrm{RL}}|, \quad \boldsymbol{k}_{\mathrm{d}} = \min(|\boldsymbol{S}_{\mathrm{RR}}|, |\boldsymbol{S}_{\mathrm{LL}}|), \quad \boldsymbol{k}_{\mathrm{h}} = \mathrm{abs}(|\boldsymbol{S}_{\mathrm{RR}}| - |\boldsymbol{S}_{\mathrm{LL}}|) \tag{8}$$

where the subscripts 's,' 'd,' and 'h' represent the surface, double-bounce, and helix scattering powers, respectively. These coherent decompositions are often used for classifying and detecting man-made targets (Alberga, Satalino, and Staykova 2008; Tamiminia et al. 2017).

The incoherent methods separate the covariance or coherency matrices into a combination of the second-order descriptors corresponding to simpler or canonical objects. The examples are Freeman-Durden decomposition parameter vectors ($\boldsymbol{P}_{\mathrm{s}}$, $\boldsymbol{P}_{\mathrm{d}}$, and $\boldsymbol{P}_{\mathrm{v}}$) and Yamaguchi decomposition parameter vectors ($\boldsymbol{P}_{\mathrm{s}}^{\mathrm{Y}}$, $\boldsymbol{P}_{\mathrm{d}}^{\mathrm{Y}}$, $\boldsymbol{P}_{\mathrm{v}}^{\mathrm{Y}}$, and $\boldsymbol{P}_{\mathrm{c}}^{\mathrm{Y}}$), which are defined as follows (Freeman and Durden 1998; Yamaguchi et al. 2005).

$$\boldsymbol{P}_{\mathrm{s}} = \boldsymbol{f}_{\mathrm{s}}\left(1 + |\boldsymbol{\beta}|^2\right), \quad \boldsymbol{P}_{\mathrm{d}} = \boldsymbol{f}_{\mathrm{d}}\left(1 + |\boldsymbol{\alpha}|^2\right), \quad \boldsymbol{P}_{\mathrm{v}} = 8\boldsymbol{f}_{\mathrm{v}}/3 \tag{9}$$

$$\boldsymbol{P}_{\mathrm{s}}^{\mathrm{Y}} = \boldsymbol{f}_{\mathrm{s}}\left(1 + |\boldsymbol{\beta}|^2\right), \quad \boldsymbol{P}_{\mathrm{d}}^{\mathrm{Y}} = \boldsymbol{f}_{\mathrm{d}}\left(1 + |\boldsymbol{\alpha}|^2\right), \quad \boldsymbol{P}_{\mathrm{v}}^{\mathrm{Y}} = \boldsymbol{f}_{\mathrm{v}}, \quad \boldsymbol{P}_{\mathrm{c}}^{\mathrm{Y}} = \boldsymbol{f}_{\mathrm{c}} \tag{10}$$

where the subscripts 'v' and 'c' represent the volume and helix scattering powers, respectively. In contrast to the coherent decompositions, these incoherent decompositions are more suitable for classifying and detecting natural targets (McNairn et al. 2009).

2.1.4. *Eigenvalues decomposition parameters*

Eigenvalues decomposition parameters, extracted from the coherency matrix, are the statistical-based features. Eigenvalues decomposition vectors ($\boldsymbol{\lambda}_1$, $\boldsymbol{\lambda}_2$, and $\boldsymbol{\lambda}_3$) are the weight indices of each scattering mechanism. Moreover, three main parameters of entropy ($\boldsymbol{H}$), anisotropy ($\boldsymbol{A}$), and alpha angle ($\bar{\boldsymbol{\alpha}}$), which are defined by these feature vectors, have shown their usefulness for land-cover classification (Entezari, Motagh, and Mansouri 2012; Deng, Yan, and Wang 2015; Tamiminia et al. 2017). $\boldsymbol{H}$, the randomness of a scattering process, is in range of [0, 1] and it represents the purity and scatter type. The value of 0 indicates a single scattering mechanism and 1 indicates a depolarizing target. $\boldsymbol{A}$ describes the contribution of scattering components. $\bar{\boldsymbol{\alpha}}$ is in range of [0°, 90°]. The value of 0° refers to surface scattering, 45° refers to dipole scattering, and 90° refers to double-bounce scattering (Hoekman, Vissers, and Tran 2011). These parameters are defined as follows (Cloude and Pottier 1997).

$$\boldsymbol{H} = -\sum_{i=1}^{3} p_i \log_3 p_i, \quad A = (\lambda_2 - \lambda_3)/(\lambda_2 + \lambda_3), \quad \bar{\boldsymbol{\alpha}} = \sum_{i=1}^{3} p_i \boldsymbol{\alpha}_i \tag{11}$$

where p_i is the normalized probability of each eigenvalue defined as (Cloude and Pottier 1997)

$$p_i = \lambda_i / \sum_{k=1}^{3} \lambda_k \tag{12}$$

The combination of $\boldsymbol{H}$ and $\boldsymbol{A}$, i.e. $\boldsymbol{HA}$, $\boldsymbol{H}(1-\boldsymbol{A})$, $(1-\boldsymbol{H})\boldsymbol{A}$, and $(1-\boldsymbol{H})(1-\boldsymbol{A})$, can be helpful in detecting the scattering mechanism of some land covers (Lee and Pottier 2009). Two other feature vectors extracted by eigenvalues of the coherency matrix are pedestal height ($\boldsymbol{\psi}$) and radar vegetation index. These are very promising for vegetation analysis and defined as follows (Samadzadegan and Ferdosi 2012).

$$\boldsymbol{\psi} = \min(\lambda_1, \lambda_2, \lambda_3)/(\lambda_1 + \lambda_2 + \lambda_3), \quad \text{RVI} = 4\lambda_3/(\lambda_1 + \lambda_2 + \lambda_3) \tag{13}$$

On the whole, the features mentioned above may be useful for discriminating some land covers and less helpful for others. Thus, this study employed all these features to have a diverse set of polarimetric features. The methods described in the next section can divide feature sets or select optimum features.

2.2. *MCSs*

There are two general approaches to designing an MCS. The first approach is the combination of different classifiers. The second approach, which is more popular, is the combination of variants of a base classifier. Boosting, bagging, and RF are well-known methods of the second approach (Du et al. 2012).

2.2.1. *Boosting*

The most widely used boosting method in machine learning literature is AdaBoost (the acronym of adaptive boosting). AdaBoost concentrates on misclassified samples.

It increases the weights of misclassified samples in each repetition. Outputs of several iterations are combined sequentially using a weighted MV (WMV) technique (Ghimire et al. 2012). The most important parameter of AdaBoost is the number of iterations (N_{Ite}).

2.2.2. *Bagging*

In bagging (the acronym of bootstrap aggregating), different subsets of training data, which are called bags, are randomly chosen with replacements from the entire training data. Then, a unique model of a base classifier is trained using each subset. Finally, outputs of these classifiers are combined in parallel using a MV technique (Ghimire et al. 2012). The number of bags (N_{Bag}) is the main parameter of bagging to be tuned.

2.2.3. *RF*

RF is a bagging in which a DT algorithm is the base classifier. Furthermore, after choosing each subset, several features are randomly selected from the entire feature set (Long et al. 2013). Thus, RF has two main parameters to be tuned: the number of trees used in the system (N_{Trees}) and the number of features to be kept in each subset (M_{Try}).

2.3. *Voting techniques*

A voting method is a procedure to combine class labels or outputs of classifiers. Two well-known voting techniques are commonly used in the literature: MV and WMV. Moreover, this article proposes an extended version of MV.

2.3.1. *MV*

The MV method, used in bagging and RF, chooses a class for a given sample, when all classifiers agree on that class, or when that class receives the highest number of votes among all votes obtained by all classifiers (Mangai et al. 2010).

2.3.2. *WMV*

Used in AdaBoost, WMV is a weighted type of MV. This method is more competent than MV for combining decisions when classifiers do not have the same performance or weights of data or classes are not equal (Mangai et al. 2010).

2.3.3. *Objective MV*

As mentioned above, MV chooses a winning class that has received the highest number of votes. However, two potential ambiguities may occur during an MV procedure. First, two or more classes may have the same largest number of votes for a given sample. This means that mode of individual decisions is non-unique. Second, no class has the largest number of votes; it means that all classifiers have decided diverse classes. Consequently, MV cannot explicitly decide for all samples. Ma et al. (2014) proposed a soft voting technique. This article proposes an extended type of MV, which aims to resolve these two ambiguities objectively by offering two practical strategies. The proposed voting technique is thus called objective MV (OMV). According to Figure 2, for sample x, the procedure of OMV may be one of the following ways.

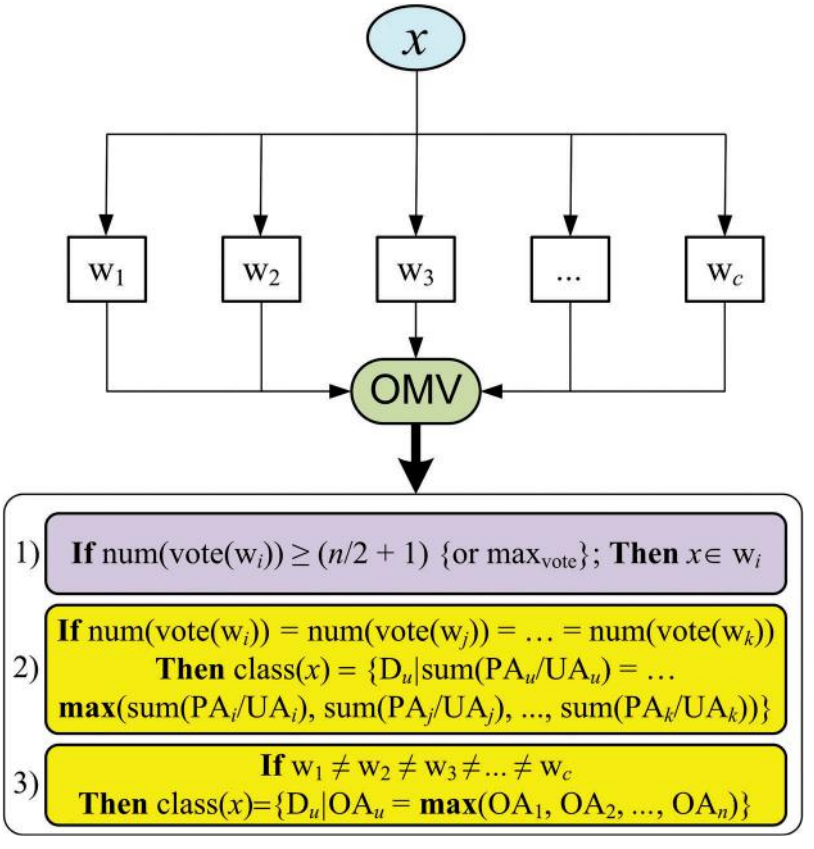

Figure 2. The procedure of OMV proposed in this article.

(1) Most of the classifiers (or $n/2 + 1$; where n is the number of all classifiers) are unanimous on class w_i. Thus, similarly to MV, x is assigned to class w_i.
(2) Two or more classes ($w_i, w_j, \ldots, w_k$; $i \neq j \neq k$; $i, j, k \in \{1, 2, 3, \ldots, c\}$; where c is the number of all classes) have the same largest number of votes. In this case, OMV decides based on the ratio of producer's accuracy (PA) to user's accuracy (UA) of classifiers for each winning class as follows: x is assigned to class obtained by D_u (decision of uth classifier, $u \in \{1, 2, 3, \ldots, n\}$), if the summation of PA_u/UA_u is maximum among all PA/UA values.
(3) All classifiers decide diverse classes for x. In this case, OMV decides based on the overall accuracy (OA) of classifiers. In fact, x is assigned to the class obtained by D_u, if OA_u is maximum among all OA values.

3. Experiments and discussion

3.1. *PolSAR data sets and preprocessing*

Three benchmark PolSAR data sets were used in this experiment. They were collected by three SAR sensors with different frequencies (X-, C-, and L-band). The study area was the San Francisco Bay, CA, USA. The X-band data were acquired by the space borne

TerraSAR-X sensor with the stripFar beams (StripMap mode). The C-band data were acquired by the space borne Radarsat-2 sensor with the FQ9 beams (single beams mode). Finally, the L-band data were acquired by the airborne AIRSAR sensor with the Stokes matrix, multi-looked cross (STK-MLC) format (PolSAR mode). All three data sets were acquired in spring months (April–May).

In the preprocessing steps, we applied multi-look processing (with the sizes of 5 × 5, 2 × 3, and 1 × 1), as well as the refined Lee filter (Lee, Grunes, and De Grandi 1999), with the sizes of 7 × 7 pixels (for X- and C-bands) and 5 × 5 pixels (for L-band), to reduce the speckle effect from the PolSAR images. The spatial resolution of the three data sets after preprocessing was in the range of 10–15 m. The Pauli RGB colour compositions and the reference data of all three data sets are shown in Figure 3.

After the preprocessing steps, training and test samples were chosen for each data set. In this study, 10, 20, and 40 samples per class were randomly stratified and selected for the training process to assess the algorithms concerning the limited training samples. The remaining samples were used as the test samples. From the reference data, three major land-cover classes including water (Wa), vegetation (Ve) (including farmland, grasslands, and forestland), and built-up (Bu) (mainly building and roads) were defined for all three data sets. Table 1 presents the number of all samples. It is noteworthy that the number of samples for all the data sets was the same.

After selecting the training samples, 49 polarimetric features, introduced in section II, were extracted from each of the three data sets (see Table 2).

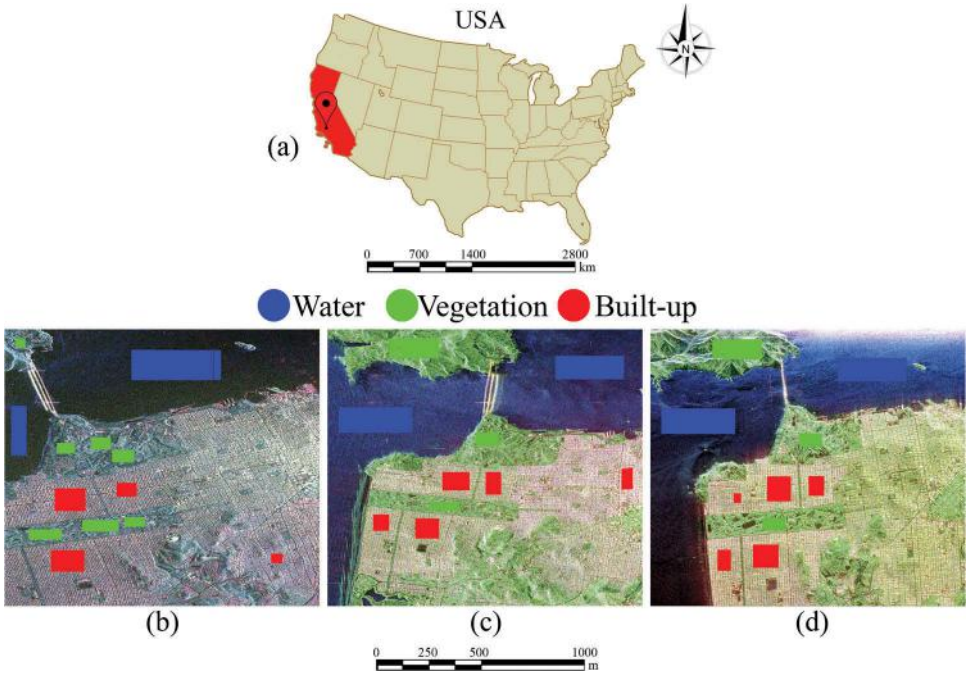

Figure 3. (a) The study of area: San Francisco Bay, CA, USA; The Pauli RGB image (blue: $|\boldsymbol{S}_{HH} + \boldsymbol{S}_{VV}|$, green: $2|\boldsymbol{S}_{HV}|$, red: $|\boldsymbol{S}_{HH} - \boldsymbol{S}_{VV}|$) and reference data of (b) X-band, (c) C-band, and (d) L-band data sets, over the San Francisco Bay, CA, USA.

Table 1. The number of samples (pixels) for three data sets.

Class	Water	Vegetation	Built-up
Number of samples	37,492	19,212	19,931
Number of training samples		{10, 20, 40}	

Table 2. Polarimetric features used in this article.

Feature name	Symbols	Number
Backscatter intensities (linear and circular)	$\sigma_{HH}, \sigma_{HV}, \sigma_{VV}, \quad \sigma_{RR}, \sigma_{RL}, \sigma_{LL}$	6
Ratio of polarizations (linear and circular)	$R_{HHVV}, R_{HVHH}, R_{HVVV}, \quad R_{RRLL}, R_{RLRR}, R_{RLLL}$	6
{\bi R}atio values (linear and circular)	$R_{HH}, R_{HV}, R_{VV}, \quad R_{RR}, R_{RL}, R_{LL}$	6
Correlation coefficients	$\rho_{HHVV}, \rho_{HVHH}, \rho_{HVVV}, \quad \rho_{RRLL}, \rho_{RLRR}, \rho_{RLLL}$	6
Coherent target decompositions	$\lvert\alpha\rvert^2, \lvert\beta\rvert^2, \lvert\gamma\rvert^2, \quad \lvert k_s\rvert^2, \lvert k_d\rvert^2, \lvert k_h\rvert^2$	6
Incoherent target decompositions	$P_s, P_d, P_v, \quad P_s^Y, P_d^Y, P_v^Y, P_c^Y$	7
Eigenvalues decompositions	$\lambda_1, \lambda_2, \lambda_3, \quad H, A, \bar{\alpha},$ $HA, H(1-A), (1-H)A, (1-A)(1-H), \quad \psi, RVI$	12

3.2. *Implementation and evaluation*

All the tests were carried out on a Windows 10 64 bit system with Intel® Core™ i7-6500 U CPU @ 2.50 GHz and 16 GB of RAM.

In this article, DT (classification and regression tree [CART] algorithm) and NN (multilayer perceptron [MLP] algorithm) were used as the base classifiers of AdaBoost and bagging. Therefore, two types of MCS methods were implemented in this article: tree-based MCSs: AdaBoost and bagging with DT (AdaDT and BaDT) and RF; and neural-based MCSs: AdaBoost and bagging with NN (AdaNN and BaNN). Three voting techniques, MV, WMV, and OMV, were also used to fuse the results of the MCSs. For the WMV, the kappa coefficient (k) obtained by each method was used as the weight of that method.

Optimum model selection for the AdaDT and AdaNN methods was accomplished based on a cross-validation strategy. By contrast, for the BaDT, BaNN, and RF methods, the out-of-bag error was used in a grid search procedure. Table 3 presents the domains of N_{Ite} for optimizing AdaDT and AdaNN, N_{Bag} for optimizing BaDT and BaNN, and N_{Trees} and M_{Try} for optimizing RF.

For evaluating the methods, well-known accuracy metrics (OA of classification, PA and UA of each class) were calculated. A high PA value for a given class indicates high efficiency of an algorithm for the classification of that class, while a high UA value implies high reliability of the results of that class obtained by the algorithm (Congalton 1991). In addition to the accuracy metrics, MCSs were also compared in terms of operating time.

3.2.1. *Comparison of MCSs and individual methods*

Table 4 shows that the MCSs obtained a higher OA than the individual DT and NN for all three training sizes for the classification of the X-band data. The difference for DT and

Table 3. The range of the main parameters for model selection of MCS methods.

Parameter	Domain
N_{Ite}, N_{Bag}, N_{Trees}	[5, 10, 20, 30, 40, 50, 60, 70, 80, 90, 100, 200, 300, 400, 500]
M_{Try}	[7, 14, 21, 28, 35, 42, 49]

Table 4. OA (%) results for three data sets..

Data	Size	DT	AdaDT	BaDT	RF	NN	AdaNN	BaNN
X-band data	10	53.25	**81.34**	67.59	74.10	51.35	**71.66**	54.87
	20	56.09	**84.16**	71.47	76.41	55.42	**73.80**	65.46
	40	61.50	**84.09**	74.87	74.55	62.79	**83.68**	70.14
	SD	4.20	1.61	3.65	**1.22**	**5.80**	6.41	7.83
C-band data	10	46.63	86.50	88.85	**94.46**	55.45	**95.25**	59.26
	20	53.88	90.94	91.07	**95.56**	76.19	**97.03**	78.77
	40	60.87	91.79	92.87	**94.62**	80.93	**97.61**	86.65
	SD	7.12	2.84	2.01	**0.59**	13.55	**1.23**	14.10
L-band data	10	43.11	68.46	83.99	**85.11**	50.04	**86.83**	55.50
	20	36.33	61.64	85.44	**90.96**	62.76	**84.84**	60.00
	40	50.24	62.15	90.18	**94.33**	69.29	**96.56**	86.14
	SD	6.95	3.80	**3.24**	4.66	9.79	**6.27**	16.54

The best results were bolded.

tree-based MCSs was in the range of 13–28% and for NN and neural-based MCSs was in the range of 3–21%.

Much higher OA values for the MCSs compared with the individual classifiers were confirmed in the classification of the C- and L-bands for all three training sizes. For example, in the classification of the C-band, the difference of the MCSs and individual methods was in the range of 5–48%. Among the MCSs, the tree-based MCSs had a higher quota. Moreover, in the classification of the L-band, the OA of the MCSs was more than 50% higher.

Table 4 presented a lower standard deviation (SD) of tree-based MCSs than DT, but a higher SD of neural-based MCSs than NN in the classification of the X-band with the three training sizes. However, in the classification of the C- and L-band data sets, SD values of all the MCSs, except for BaNN, were lower compared with the individual classifiers. These results pointed out more stable results of the MCSs than the individual classifiers in the classification of the three PolSAR data sets. This conclusion was consistent with previous studies, which stated that these two classifiers, i.e. DT and NN, are unstable and weak classifiers (Breiman 1996; Polikar 2006; Du et al. 2012).

In terms of producer and user accuracies, both tree-based and neural-based MCSs, except for BaNN in some cases, have obtained higher mean-PA and mean-UA values (over the classes) compared with DT and NN, respectively (see Tables 5 and 6). This difference exceeded 50%.

In the classification of the X-band, DT had a problem in the detection of the built-up class; tree-based MCSs obtained around 15–50% higher PA values. DT also had a low UA value in the detection of vegetation. By contrast, tree-based MCSs were more reliable with 5–40% higher UA values. In another case, NN had an extreme problem in the detection of vegetation (especially for the size of 20), whereas neural-based MCSs obtained 10–70% higher PA values. Where NN had a low UA value in the detection of water, neural-based MCSs were more reliable with 10–35% higher UA values. In another instance, where DT detected less than half of vegetation from C-band, tree-based MCSs were more efficient and more reliable with 51% higher PA and 41% higher UA values. Furthermore, AdaNN obtained 78% higher PA and 52% higher UA values than NN in the detection of built-up areas and vegetation, respectively.

PA and UA results for the MCSs were more impressive in the classification of the L-band. DT had less than 51% PA and UA values in the classification with the size of 10,

Table 5. PA (%) results for three data sets.

		10				20				40			
Data	Method	Wa	Ve	Bu	Mean	Wa	Ve	Bu	Mean	Wa	Ve	Bu	Mean
X-band data	DT	65.67	**61.06**	22.33	49.69	87.72	20.96	30.44	46.37	77.31	60.71	32.54	56.85
	AdaDT	97.00	57.65	**74.72**	**76.46**	99.37	**63.08**	**75.86**	**79.44**	99.71	**61.31**	**76.68**	**79.23**
	BaDT	**100.00**	30.87	42.01	57.63	**100.00**	43.30	44.96	62.75	**100.00**	45.93	55.50	67.14
	RF	99.93	47.40	51.23	66.19	99.71	60.16	48.23	69.37	**100.00**	40.90	59.12	66.67
	NN	**90.00**	10.08	18.43	39.50	91.06	0.90	40.92	44.29	91.17	14.86	55.59	53.87
	AdaNN	82.77	**76.63**	**81.04**	**80.06**	81.00	**71.76**	**87.34**	**80.04**	86.85	**82.26**	**95.95**	**88.36**
	BaNN	73.07	23.86	50.52	49.15	**99.97**	11.12	52.95	54.68	**99.46**	25.95	57.60	61.00
C-band data	DT	55.29	44.94	31.99	44.07	54.34	59.99	47.11	53.81	66.17	62.86	48.99	59.34
	AdaDT	99.83	91.49	56.60	82.64	99.87	94.59	70.59	88.35	98.91	95.04	75.27	89.74
	BaDT	**100.00**	**95.34**	61.64	85.66	**99.94**	**97.95**	67.72	88.54	99.99	**98.23**	74.31	90.84
	RF	99.99	93.63	**84.84**	**92.82**	99.66	96.62	**86.81**	**94.36**	**100.00**	97.80	**81.45**	**93.08**
	NN	57.74	49.32	57.07	54.71	**100.00**	91.03	17.10	69.38	**100.00**	87.23	38.99	75.41
	AdaNN	**99.91**	**92.30**	**89.34**	**93.85**	99.72	**93.80**	**95.08**	**96.20**	99.94	95.99	**94.80**	**96.91**
	BaNN	82.03	36.80	38.07	52.30	99.99	90.03	28.01	72.68	99.84	**98.06**	50.85	82.91
L-band data	DT	37.83	46.65	49.61	44.70	16.83	66.33	44.09	42.42	46.24	66.12	42.48	51.61
	AdaDT	73.77	59.61	67.00	66.79	57.73	49.16	**81.02**	62.64	42.87	72.21	**88.72**	67.93
	BaDT	**98.42**	**83.96**	56.87	79.75	98.66	93.11	53.16	81.64	**98.67**	**98.22**	66.45	87.78
	RF	93.60	72.49	**81.32**	**82.47**	**98.77**	**93.87**	73.45	**88.70**	97.14	97.38	86.12	**93.55**
	NN	78.84	43.33	2.34	41.50	73.37	71.98	33.94	59.76	70.34	89.45	47.89	69.23
	AdaNN	**98.29**	**74.15**	**95.12**	**89.19**	**90.66**	**83.11**	**93.10**	**88.96**	**99.64**	**92.12**	**96.42**	**96.06**
	BaNN	72.99	47.40	30.40	50.26	69.73	67.53	34.41	57.23	88.69	87.38	68.27	81.45

The best results were bolded.

Table 6. UA (%) results for three data sets.

		10				20				40			
Data	Method	Wa	Ve	Bu	Mean	Wa	Ve	Bu	Mean	Wa	Ve	Bu	Mean
X-band data	DT	81.10	43.18	88.40	70.12	57.26	65.95	72.21	65.14	80.10	39.07	91.55	70.24
	AdaDT	**85.76**	**77.72**	93.24	**85.57**	**87.49**	**80.30**	92.36	**86.72**	**87.31**	**82.72**	91.09	**87.04**
	BaDT	68.83	53.50	**97.29**	73.21	73.59	60.06	**97.69**	77.11	75.17	61.71	**98.17**	78.35
	RF	78.24	63.16	91.93	77.78	81.89	69.87	91.61	81.12	74.65	65.82	97.02	79.16
	NN	46.91	73.63	**89.63**	69.66	59.50	62.50	80.08	67.36	65.44	74.73	94.84	78.33
	AdaNN	**82.77**	**76.63**	81.04	**80.06**	**81.00**	**71.76**	**87.34**	**80.04**	**86.85**	**82.26**	**95.95**	**88.36**
	BaNN	73.25	31.45	76.04	62.67	67.25	68.65	84.64	73.68	74.79	66.71	88.91	76.80
C-band data	DT	54.40	47.33	81.36	61.03	65.86	61.20	63.58	63.54	77.35	54.38	84.61	72.12
	AdaDT	93.15	75.70	98.14	89.00	91.10	**90.13**	98.62	93.28	94.94	84.48	95.79	91.74
	BaDT	93.62	79.57	**99.03**	90.74	98.71	79.37	**98.67**	92.25	**99.69**	82.14	98.55	93.46
	RF	**96.18**	**88.62**	98.77	**94.52**	**99.01**	88.59	98.04	**95.22**	99.05	**84.88**	**98.75**	**94.23**
	NN	76.51	41.18	86.37	64.94	79.45	79.02	**99.44**	85.97	89.28	73.75	95.10	86.04
	AdaNN	**97.51**	**93.13**	**95.42**	**95.36**	**98.76**	**97.12**	94.64	**96.84**	**98.49**	**96.61**	97.48	**97.53**
	BaNN	76.16	53.93	60.71	63.27	84.90	78.22	98.22	87.12	94.85	74.79	**98.81**	89.48
L-band data	DT	51.66	46.92	48.34	48.97	49.35	39.49	60.52	49.79	73.32	39.36	60.21	57.63
	AdaDT	**99.33**	46.79	63.79	69.97	91.38	62.07	58.77	70.74	96.30	49.70	70.34	72.11
	BaDT	**96.50**	71.03	**93.87**	87.14	**99.40**	71.75	95.25	88.80	**99.43**	75.52	**98.85**	91.27
	RF	92.13	**84.64**	89.69	**88.82**	98.99	**81.81**	**95.67**	**92.16**	99.19	**86.28**	96.15	**93.87**
	NN	66.26	57.71	84.60	70.08	79.51	50.08	84.36	71.32	89.83	56.30	83.75	76.63
	AdaNN	**98.29**	**74.15**	**95.12**	**89.19**	**90.66**	**83.11**	**93.10**	**88.96**	**99.64**	**92.12**	**96.42**	**96.06**
	BaNN	75.28	47.16	81.89	66.49	76.56	74.41	77.95	75.20	96.59	75.41	87.89	85.51

The best results were bolded.

while tree-based MCSs obtained up to 50% higher PA and UA values. NN was also inefficient in the detection of built-up with less than 50% PA, for example with a PA value of about 2% for the size of 10. However, neural-based MCSs obtained 28–93% higher PA values in the detection of this class.

To explain the reasons for the superiority of MCSs over individual methods, some facts about MCSs are refereed. Both DT and NNs have a rather simpler, weaker structure

for the classification task. By contrast, MCSs, which have a more complex architecture, use some strategies to divide and conquer big data. These strategies include resampling of data, reweighing of data, and selecting the optimum features that lead to creating a diversity among several individual classifiers, to reduce the risk error of choosing every single classifier and to improve the performance of their ensemble.

3.2.2. *Comparison of tree-based and neural-based MCSs*

AdaDT and RF, among tree-based MCSs and AdaNN, among neural-based MCSs, obtained the highest OA in the classification of the three data sets. Furthermore, AdaNN has higher OA, mean-PA, and mean-UA values than tree-based MCSs in the classification of the C- and L-bands and *vice versa* in the classification of the X-band.

Regarding robustness, RF had the highest stability in the classification of the X- and C-bands. In the classification of the L-band, BaDT was the most stable MCS method, whereas BaNN had the lowest stability in the classification of all three data sets.

BaNN has the lowest efficiency (lower PA values), lowest reliability (lower UA values), and lowest stability (higher SD values) among all the MCSs for the classification of all three data sets.

Figures 4(a)–(c) show the operating times of the MCSs in the classification of the X-, C-, and L-band data sets for the three training sizes. This time was calculated during training, optimization, and testing processes for each algorithm. These figures demonstrated that operating times of tree-based MCSs were much lower compared with neural-based MCSs in the classification of the three data sets for the three training sizes. This advantage is due to the faster execution of the CART algorithm compared with the MLP algorithm. In fact, CART calculates information gain between features and classes, which is not a time-consuming action. MLP, in contrast to CART, is a black-box algorithm that may map data into another feature space. It can be a time-consuming action.

Among the MCSs, AdaNN had the highest operating time in the classification of the X- and C-band data sets for the three training sizes. Moreover, in the classification of the L-band data, BaNN had the highest operating time for the size of 40. BaDT had the lowest time in the classification of all three data sets for the three training sizes. Thus, it could be concluded that bagging was usually faster than its competitors, i.e. AdaBoost. This fact could be due to the simpler and faster structure of bagging than AdaBoost, which confirms previous reports (Breiman 2001; Du et al. 2012). After BaDT, RF had the lowest operating time in the classification of all three data sets for the three training sizes. It is noteworthy that the time of testing RF was lower than the time of testing bagging algorithms, due to fewer features being used in RF compared with bagging.

3.2.3. *Comparison of frequency band efficiency*

Figures 5(a)–(c) show the best classification maps of tree-based and neural-based MCSs for the three data sets. Analysing these figures allows to demonstrate that the maps of MCSs obtained from the C-band (Figure 5(b)) had more homogeneous and more uniform appearances compared with the L- and X-bands (Figures 5(a) and (c)). The maps obtained from the L-band were smoother than those obtained from X-band. The land-cover maps obtained from the X-band were rather unfavourable, especially those obtained by neural-based MCSs (such as BaNN). A lot of mixed pixels could be observed inside of vegetation or built-up areas in these maps.

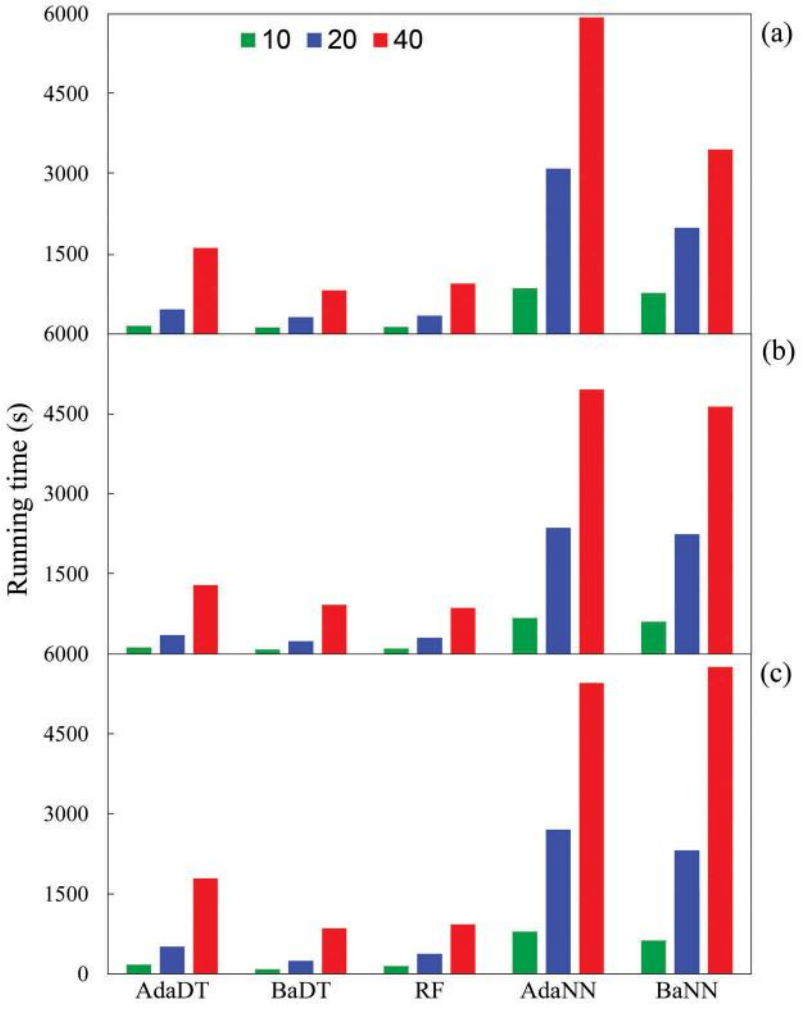

Figure 4. Operating time plots of tree-based and neural-based MCSs for (a) X-band, (b) C-band, and (c) L-band data sets.

Figures 6(a) and (b) show the PA and UA values of the MCSs averaged over the three training sizes. The mean-PA and mean-UA values (averaged over classes) of all the MCSs obtained from the C-band were higher than those obtained from the L- and X-bands. Furthermore, the values of all the MCSs, except for AdaDT, obtained from the L-band were higher than those obtained from the X-band.

To sum up, in the classification of water, tree-based MCSs were more efficient in the X-band and the C-band (higher PA); however, they were more reliable in the L-band and then C-band (higher UA). By contrast, neural-based MCSs were more efficient and more reliable in the C-band.

In the classification of vegetation, both tree-based and neural-based MCSs were more efficient and more reliable in the C-band. Meanwhile, the results of the L-band were more effective and more reliable, except for the results of AdaDT, compared with the X-band.

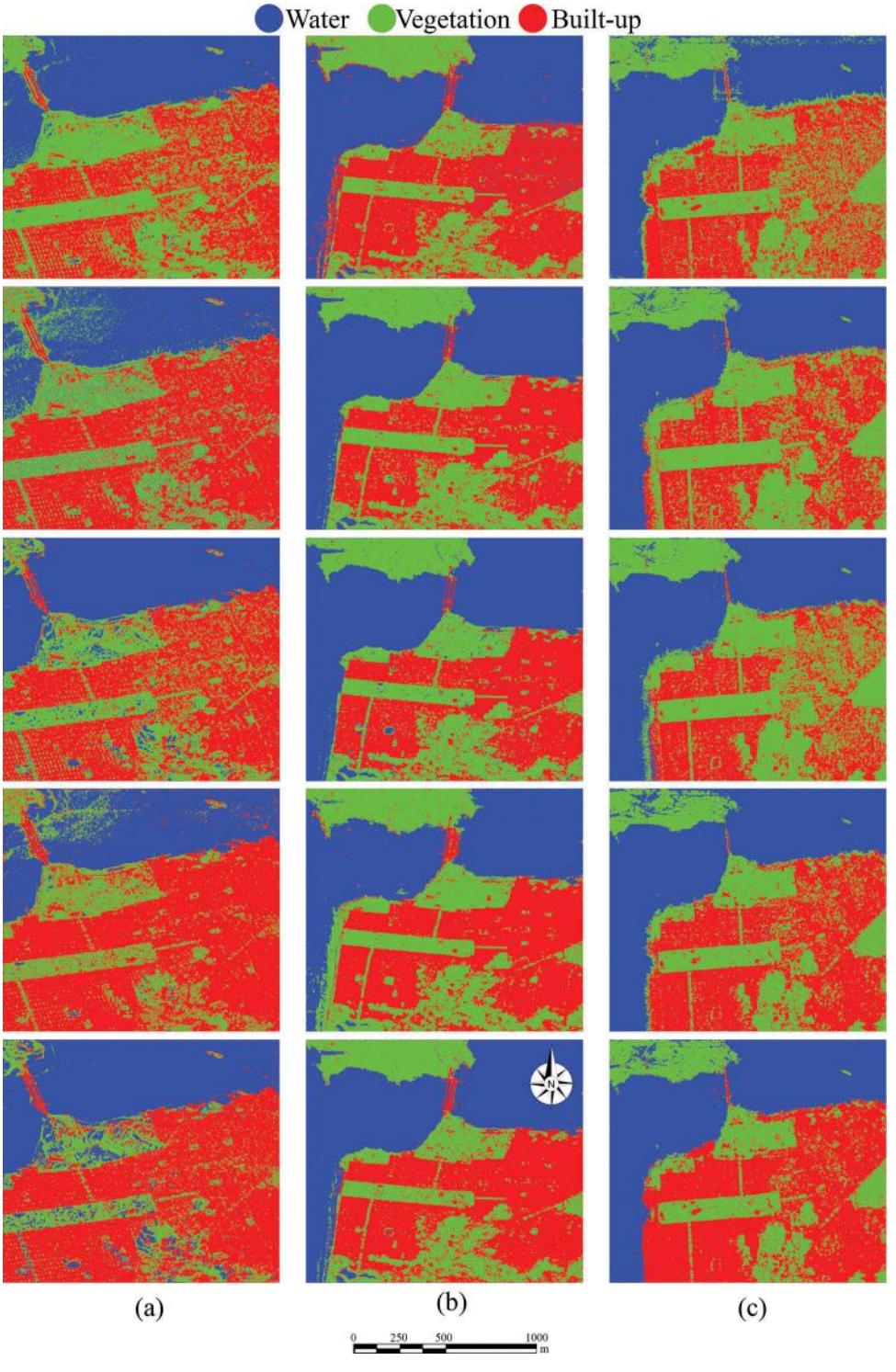

Figure 5. Classification maps of AdaDT, BaDT, RF, AdaNN, and BaNN (top-down) for (a) X-band, (b) C-band, and (c) L-band data sets.

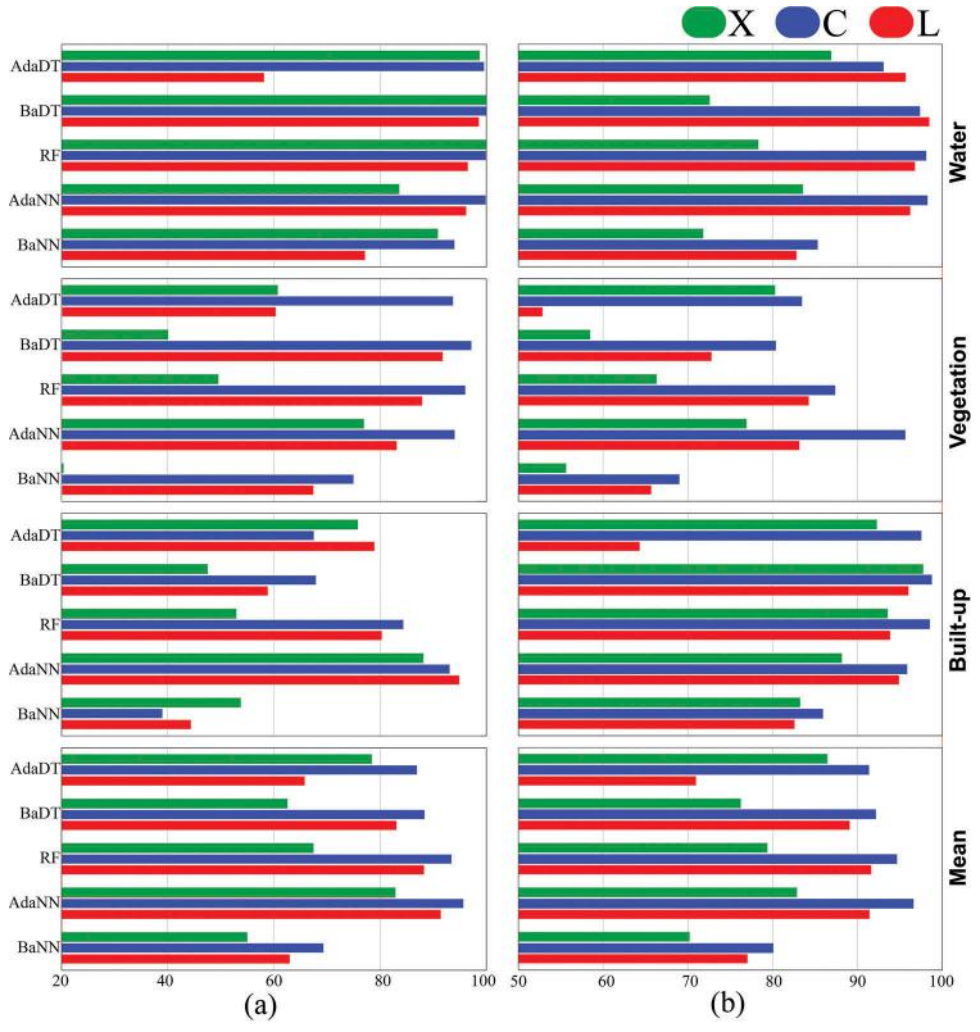

Figure 6. (a) PA and (b) UA values obtained by MCSs averaged over three training sizes in the classification of X-, C-, and L-band data sets.

In the classification of built-up areas, some of the MCSs were more efficient in the X-band, such as BaNN; some were more efficient in the C-band, such as BaDT and RF; and some were more efficient in the L-band, such as AdaDT and AdaNN. All the MCSs had also higher reliability in the classification of the C-band.

Accordingly, Figures 5 and 6 confirmed that the results of the C-band are better than the results of the L-band and subsequently better than the X-band for land-cover mapping in the study area.

The above conclusion can be satisfied from Figure 7. The scatter plots (for the three linear polarizations) of the three classes in the C-band data were distinct from each other (see Figure 7(b)). By contrast, they were overlapping for the X- and L-bands (see Figures 7(a) and (c)). Meanwhile, in the X-band, the scatter plots of water and built-up areas had more overlap than in the L-band.

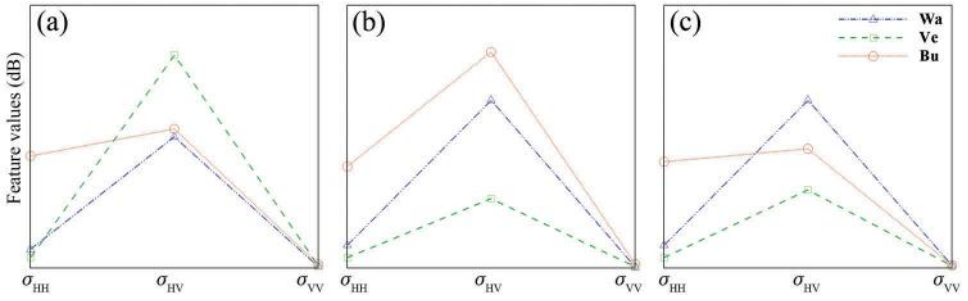

Figure 7. Scatter plots of linear polarizations for (a) X-band, (b) C-band, and (c) L-band data sets.

3.2.4. *Comparison of voting techniques*

Table 7 presents the results of the voting methods averaged over the three training sizes. The proposed OMV obtained higher mean-OA, mean-PA, and mean-UA values than both MV and WMV in the classification of all three PolSAR data sets. Mean accuracy values of OMV were also often higher than all or most of the MCSs. For example, in the classification of the C-band, OMV was more successful than all the MCSs.

The differences between the results of OMV and MV were 1–4% in the classification of the three data sets. OMV obtained 0.3–2% higher accuracy values than the WMV.

Regarding robustness, in the classification of X-band, WMV had the most stable OA results (lower SD of OA). By contrast, MV and OMV had the most stable OA in the classification of the C- and L-band data sets, respectively. However, the results of OMV were in general more stable than those of the two other voting techniques.

4. Conclusion

The capability of MCSs for land-cover mapping from PolSAR Earth observations with limited training samples was studied in this article. Two popular types of MCSs, tree-based MCSs (AdaDT, BaDT, and RF) and neural-based MCSs (AdaNN and BaNN), were used for the classification of three benchmark PolSAR data sets. These data sets had different frequencies of X, C, and L, which were collected in the San Francisco Bay, CA, USA. The results of the MCSs were combined using three voting techniques: MV, WMV, and a newly proposed method, namely OMV.

Both tree-based and neural-based MCSs had higher capability (higher OA), efficiency (higher PA), and reliability (higher UA) than DT and NN in the classification of the three

Table 7. OA, PA, and UA (%) results of voting techniques averaged over three training sizes.

		X-band data				C-band data				L-band data			
		Wa	Ve	Bu	Mean	Wa	Ve	Bu	Mean	Wa	Ve	Bu	Mean
MV	PA	**100.00**	36.58	81.88	72.82	**100.00**	98.47	87.18	95.22	**98.87**	98.14	91.04	96.02
	UA	73.59	78.17	**99.05**	83.60	99.09	88.77	**99.39**	95.75	99.11	90.04	**99.45**	96.20
	OA	79.39	3.04			96.28	**0.35**			96.65	1.93		
WMV	PA	**100.00**	39.67	**88.99**	76.22	**100.00**	98.44	89.94	96.12	98.80	98.49	95.36	97.55
	UA	75.83	**82.46**	98.89	85.73	99.41	90.74	99.24	96.47	99.47	93.50	99.29	97.42
	OA	82.01	**2.00**			96.93	0.73			97.83	0.82		
OMV	PA	**100.00**	**46.84**	87.99	**78.28**	**100.00**	**98.65**	**91.67**	**96.77**	98.75	**98.83**	**96.20**	**97.93**
	UA	**78.21**	82.45	98.79	**86.48**	**99.55**	**92.21**	99.22	**96.99**	**99.66**	**94.12**	99.30	**97.69**
	OA	**83.55**	2.18			**97.49**	0.42			**98.11**	**0.39**		

data sets with limited training samples. Among MCSs, tree-based MCSs were more efficient, reliable, and stable (lower SD) than neural-based MCSs in the classification of the three PolSAR data sets. Furthermore, they performed much faster than neural-based MCSs. BaNN obtained the worst outputs with lower accuracy and lower reliability despite a higher operating time. Accordingly, we recommend and prefer tree-based MCSs in the classification of big data because of their increased accuracy and decreased operating time.

Another remarkable conclusion of this article concerned RF: it was more efficient and more reliable than its equivalent method, BaDT. Compared with its competitor, AdaDT, RF also had higher efficiency, reliability, and stability in the classification of two of the three data sets. Meanwhile, it was nearly as fast as BaDT and was much faster than AdaDT in the classification of the three PolSAR data sets. Thus, RF can be recommended as a stable, accurate, reliable, simple, and fast MCS method in the classification of PolSAR data.

Of the voting techniques investigated, the newly proposed OMV had, in most cases, higher overall, producer's and user's accuracies than its competitors, MV and WMV and all MCSs. Moreover, it was often more stable than other voting techniques. This article therefore proposes OMV as a more appropriate and objective alternative to MV for combining results of similar or various classifiers.

Comparison analysis also reported that the results obtained in the C-band data set were more accurate and reliable compared with the L- and X-band data sets for land-cover mapping in the study area. This idea can be used in further research for other scenarios, for example in agriculture, where we could choose the best polarimetric feature and the best frequency for each growth stage of crop types.

To make a fair comparison among the three benchmark PolSAR data sets, they were collected in the same season and had similar spatial resolutions. Nonetheless, other factors such as SAR acquisition modes, properties, and parameters (e.g. incident angle, steering angle, pulse length, look direction, and speed of sensor) can affect imaging and, subsequently, land-cover classification results.

Several satellite SAR sensors with different frequencies are under development. Since the results of these MCSs are relatively acceptable and accurate, they can present an operational and efficient framework for land-cover mapping applications from these sensors.

Acknowledgements

The authors would like to thank the JPL NASA, the MacDonald, Dettwiler and Associates Ltd., and the German DLR for the PolSAR data used in this research.

Disclosure statement

No potential conflict of interest was reported by the authors.

References

Alberga, V. 2007. "A Study of Land Cover Classification Using Polarimetric SAR Parameters." *International Journal of Remote Sensing* 28 (17): 3851–3870. doi:10.1080/01431160601075541.

Alberga, V., G. Satalino, and D. K. Staykova. 2008. "Comparison of Polarimetric SAR Observables in Terms of Classification Performance." *International Journal of Remote Sensing* 29 (14): 4129–4150. doi:10.1080/01431160701840182.

Breiman, L. 1996. "Bagging Predictors." *Machine Learning* 24 (2): 123–140. doi:10.1007/BF00058655.

Breiman, L. 2001. "Random Forests." *Machine Learning* 45 (1): 5–32. doi:10.1023/A:1010933404324.

Bruzzone, L., M. Marconcini, U. Wegmuller, and A. Wiesmann. 2004. "An Advanced System for the Automatic Classification of Multitemporal SAR Images." *IEEE Transactions on Geoscience and Remote Sensing* 42 (6): 1321–1334. doi:10.1109/TGRS.2004.826821.

Chen, K. S., W. P. Huang, D. H. Tsay, and F. Amar. 1996. "Classification of Multifrequency Polarimetric SAR Imagery Using a Dynamic Learning Neural Network." *IEEE Transactions on Geoscience and Remote Sensing* 34 (3): 814–820. doi:10.1109/36.499786.

Cloude, S. R., and E. Pottier. 1996. "A Review of Target Decomposition Theorems in Radar Polarimetry." *IEEE Transactions on Geoscience and Remote Sensing* 34 (2): 498–518. doi:10.1109/36.485127.

Cloude, S. R., and E. Pottier. 1997. "An Entropy Based Classification Scheme for Land Applications of Polarimetric SAR." *IEEE Transactions on Geoscience and Remote Sensing* 35 (1): 68–78. doi:10.1109/36.551935.

Congalton, R. G. 1991. "A Review of Assessing the Accuracy of Classifications of Remotely Sensed Data." *Remote Sensing of Environment* 37 (1): 35–46. doi:10.1016/0034-4257(91)90048-B.

Deng, L., Y. N. Yan, and C. Wang. 2015. "Improved POLSAR Image Classification by the Use of Multi-Feature Combination." *Remote Sensing* 7 (4): 4157–4177. doi:10.3390/rs70404157.

Deschamps, B., H. McNairn, J. Shang, and X. Jiao. 2012. "Towards Operational Radar-Only Crop Type Classification: Comparison of a Traditional Decision Tree with a Random Forest Classifier." *Canadian Journal of Remote Sensing* 38 (1): 60–68. doi:10.5589/m12-012.

Du, P., A. Samat, P. Gamba, and X. Xie. 2014. "Polarimetric SAR Image Classification by Boosted Multiple-Kernel Extreme Learning Machines with Polarimetric and Spatial Features." *International Journal of Remote Sensing* 35 (23): 7978–7990. doi:10.1080/2150704X.2014.978952.

Du, P., J. Xia, W. Zhang, K. Tan, Y. Liu, and S. Liu. 2012. "Multiple Classifier System for Remote Sensing Image Classification: A Review." *Sensors* 12 (4): 4764–4792. doi:10.3390/s120404764.

Dubois, P., J. Van Zyl, and T. Engman. 1995. "Measuring Soil Moisture with Imaging Radars." *IEEE Transactions on Geoscience and Remote Sensing* 33 (4): 915–926. doi:10.1109/36.406677.

Entezari, I., M. Motagh, and B. Mansouri. 2012. "Comparison of the Performance of L-Band Polarimetric Parameters for Land Cover Classification." *Canadian Journal of Remote Sensing* 38 (5): 629–643. doi:10.5589/m12-051.

Ferrazzoli, P., L. Guerriero, and G. Schiavon. 1999. "Experimental and Model Investigation on Radar Classification Capability." *IEEE Transactions on Geoscience and Remote Sensing* 37 (2): 960–968. doi:10.1109/36.752214.

Ferrazzoli, P., S. Paloscia, P. Pampaloni, G. Schiavon, S. Sigismondi, and D. Solimini. 1997. "The Potential of Multifrequency Polarimetric SAR in Assessing Agricultural and Arboreous Biomass." *IEEE Transactions on Geoscience and Remote Sensing* 35 (1): 5–17. doi:10.1109/36.551929.

Freeman, A., and S. L. Durden. 1998. "A Three-Component Scattering Model for Polarimetric SAR Data." *IEEE Transactions on Geoscience and Remote Sensing* 36 (3): 963–973. doi:10.1109/36.673687.

Gens, R. 2008. "Oceanographic Applications of SAR Remote Sensing." *GIScience & Remote Sensing* 45 (3): 275–305. doi:10.2747/1548-1603.45.3.275.

Ghimire, B., J. Rogan, V. R. Galiano, P. Panday, and N. Neeti. 2012. "An Evaluation of Bagging, Boosting, and Random Forests for Land-Cover Classification in Cape Cod, Massachusetts, USA." *GIScience & Remote Sensing* 49 (5): 623–643. doi:10.2747/1548-1603.49.5.623.

Habibi, M., M. R. Sahebi, Y. Maghsoudi, and S. Ghayourmanesh. 2016. "Classification of Polarimetric SAR Data Based on Object-Based Multiple Classifiers for Urban Land-Cover." *Journal of the Indian Society of Remote Sensing* 44 (6): 855–863. doi:10.1007/s12524-016-0558-5.

Hara, Y., R. G. Atkins, S. H. Yueh, R. T. Shin, and J. A. Kong. 1994. "Application of Neural Networks to Radar Image Classification." *IEEE Transactions on Geoscience and Remote Sensing* 32 (1): 100–109. doi:10.1109/36.285193.

Hoekman, D. H., M. A. Vissers, and T. N. Tran. 2011. "Unsupervised Full-Polarimetric SAR Data Segmentation as a Tool for Classification of Agricultural Areas." *IEEE Journal of Selected Topics in*

Applied Earth Observations and Remote Sensing 4 (2): 402–411. doi:10.1109/JSTARS.2010.2042280.

Huang, X., J. Wang, J. Shang, C. Liao, and J. Liu. 2017. "Application of Polarization Signature to Land Cover Scattering Mechanism Analysis and Classification Using Multi-Temporal C-Band Polarimetric RADARSAT-2 Imagery." *Remote Sensing of Environment* 193: 11–28. doi:10.1016/j.rse.2017.02.014.

Inoue, Y., T. Kurosu, H. Maeno, S. Uratsuka, T. Kozu, K. Dabrowska-Zielinska, and J. Qi. 2002. "Season-Long Daily Measurements of Multifrequency (Ka, Ku, X, C, and L) and Full-Polarization Backscatter Signatures over Paddy Rice Field and Their Relationship with Biological Variables." *Remote Sensing of Environment* 81 (2–3): 194–204. doi:10.1016/S0034-4257(01)00343-1.

Krogager, E. 1990. "New Decomposition of the Radar Target Scattering Matrix." *Electronics Letters* 26 (18): 1525–1527. doi:10.1049/el:19900979.

Lardeux, C., P. L. Frison, C. Tison, J. C. Souyris, B. Stoll, B. Fruneau, and J. P. Rudant. 2009. "Support Vector Machine for Multifrequency SAR Polarimetric Data Classification." *IEEE Transactions on Geoscience and Remote Sensing* 47 (12): 4143–4152. doi:10.1109/TGRS.2009.2023908.

Lee, J. S., M. R. Grunes, and G. De Grandi. 1999. "Polarimetric SAR Speckle Filtering and Its Implication for Classification." *IEEE Transactions on Geoscience and Remote Sensing* 37 (5): 2363–2373. doi:10.1109/36.789635.

Lee, J. S., M. R. Grunes, and R. Kwok. 1994. "Classification of Multi-Look Polarimetric SAR Imagery Based on Complex Wishart Distribution." *International Journal of Remote Sensing* 15 (11): 2299–2311. doi:10.1080/01431169408954244.

Lee, J. S., and E. Pottier. 2009. *Polarimetric Radar Imaging: From Basics to Applications*. Boca Raton, FL: CRC press. doi:10.1201/9781420054989

Liu, C., J. Yin, J. Yang, and W. Gao. 2015. "Classification of Multi-Frequency Polarimetric SAR Images Based on Multi-Linear Subspace Learning of Tensor Objects." *Remote Sensing* 7 (7): 9253–9268. doi:10.3390/rs70709253.

Long, J. A., R. L. Lawrence, M. C. Greenwood, L. Marshall, and P. R. Miller. 2013. "Object-Oriented Crop Classification Using Multitemporal ETM+ SLC-Off Imagery and Random Forest." *GIScience & Remote Sensing* 50 (4): 418–436.

Lonnqvist, A., Y. Rauste, M. Molinier, and T. Hame. 2010. "Polarimetric SAR Data in Land Cover Mapping in Boreal Zone." *IEEE Transactions on Geoscience and Remote Sensing* 48 (10): 3652–3662. doi:10.1109/TGRS.2010.2048115.

Ma, X., H. Shen, J. Yang, L. Zhang, and P. Li. 2014. "Polarimetric-Spatial Classification of SAR Images Based on the Fusion of Multiple Classifiers." *IEEE Journal of Selected Topics in Applied Earth Observations and Remote Sensing* 7 (3): 961–971. doi:10.1109/JSTARS.2013.2265331.

Maghsoudi, Y., M. Collins, and D. G. Leckie. 2012. "Polarimetric Classification of Boreal Forest Using Nonparametric Feature Selection and Multiple Classifiers." *International Journal of Applied Earth Observation and Geoinformation* 19: 139–150. doi:10.1016/j.jag.2012.04.015.

Mangai, U. G., S. Samanta, S. Das, and P. R. Chowdhury. 2010. "A Survey of Decision Fusion and Feature Fusion Strategies for Pattern Classification." *IETE Technical Review* 27 (4): 293–307. doi:10.4103/0256-4602.64604.

McNairn, H., A. Kross, D. Lapen, R. Caves, and J. Shang. 2014. "Early Season Monitoring of Corn and Soybeans with TerraSAR-X and RADARSAT-2." *International Journal of Applied Earth Observation and Geoinformation* 28: 252–259. doi:10.1016/j.jag.2013.12.015.

McNairn, H., J. Shang, X. Jiao, and C. Champagne. 2009. "The Contribution of ALOS PALSAR Multipolarization and Polarimetric Data to Crop Classification." *IEEE Transactions on Geoscience and Remote Sensing* 47 (12): 3981–3992. doi:10.1109/TGRS.2009.2026052.

Mehta, R. L., N. Parihar, A. Sinha, B. P. Shastri, and M. Chakraborty. 2014. "Discrimination between Babul Plantations and Mustard Crop Using Polarimetric C–And L–Band Data." *Journal of the Indian Society of Remote Sensing* 42 (2): 439–444. doi:10.1007/s12524-013-0319-7.

Mishra, P., D. Singh, and Y. Yamaguchi. 2011. "Land Cover Classification of PALSAR Images by Knowledge Based Decision Tree Classifier and Supervised Classifiers Based on SAR Observables." *Progress In Electromagnetics Research B* 30: 47–70. doi:10.2528/PIERB11011405.

Mountrakis, G., J. Im, and C. Ogole. 2011. "Support Vector Machines in Remote Sensing: A Review." *ISPRS Journal of Photogrammetry and Remote Sensing* 66 (3): 247–259. doi:10.1016/j.isprsjprs.2010.11.001.

Niu, X., and Y. Ban. 2014. "A Novel Contextual Classification Algorithm for Multitemporal Polarimetric SAR Data." *IEEE Geoscience and Remote Sensing Letters* 11 (3): 681–685. doi:10.1109/LGRS.2013.2274815.

Polikar, R. 2006. "Ensemble Based Systems in Decision Making." *IEEE Circuits and Systems Magazine* 6 (3): 21–45. doi:10.1109/MCAS.2006.1688199.

Qi, Z., A. G. O. Yeh, X. Li, and X. Zhang. 2015. "A Three-Component Method for Timely Detection of Land Cover Changes Using Polarimetric SAR Images." *ISPRS Journal of Photogrammetry and Remote Sensing* 107: 3–21. doi:10.1016/j.isprsjprs.2015.02.004.

Rignot, E. J., S. J. Ostro, J. J. Van Zyl, and K. C. Jezek. 1993. "Unusual Radar Echoes from the Greenland Ice Sheet." *Science* 261: 1710–1713. doi:10.1126/science.261.5129.

Rosenthal, W. D., B. J. Blanchard, and A. J. Banchrd. 1985. "Visible/IR/Microwave Agricultural Classification, Biomass and Plant Height Algorithms." *IEEE Transactions on Geoscience and Remote Sensing* GE-23: 84–90. doi:10.1109/TGRS.1985.289404.

Salehi, M., M. R. Sahebi, and Y. Maghsoudi. 2014. "Improving the Accuracy of Urban Land Cover Classification Using Radarsat-2 PolSAR Data." *IEEE Journal of Selected Topics in Applied Earth Observations and Remote Sensing* 7 (4): 1394–1401. doi:10.1109/JSTARS.2013.2273074.

Samadzadegan, F., and E. Ferdosi. 2012. "Classification of Polarimetric SAR Images Based on Optimum SVMs Classifier Using Bees Algorithm." *Polarization* 6 (9): 1–10.

Shah Hosseini, R., I. Entezari, S. Homayouni, M. Motagh, and B. Mansouri. 2011. "Classification of Polarimetric SAR Images Using Support Vector Machines." *Canadian Journal of Remote Sensing* 37 (2): 220–233. doi:10.5589/m11-029.

Shokrollahi, M., and H. Ebadi. 2016. "Improving the Accuracy of Land Cover Classification Using Fusion of Polarimetric SAR and Hyperspectral Images." *Journal of the Indian Society of Remote Sensing* 44 (6): 1017–1024. doi:10.1007/s12524-016-0559-4.

Souissi, B., M. Ouarzeddine, and A. Belhadj-Aissa. 2014. "Optimal SVM Classification for Compact Polarimetric Data Using Stokes Parameters." *Journal of Mathematical Modelling and Algorithms in Operations Research* 13 (4): 433–446. doi:10.1007/s10852-013-9244-6.

Tamiminia, H., S. Homayouni, H. McNairn, and A. Safari. 2017. "A Particle Swarm Optimized Kernel-Based Clustering Method for Crop Mapping from Multi-Temporal Polarimetric L-Band SAR Observations." *International Journal of Applied Earth Observation and Geoinformation* 58: 201–212. doi:10.1016/j.jag.2017.02.010.

Uhlmann, S., and S. Kiranyaz. 2014. "Integrating Color Features in Polarimetric SAR Image Classification." *IEEE Transactions on Geoscience and Remote Sensing* 52 (4): 2197–2216. doi:10.1109/TGRS.2013.2258675.

Van Zyl, J. J., and C. F. Burnette. 1992. "Bayesian Classification of Polarimetric SAR Images Using Adaptive A Priori Probabilities." *International Journal of Remote Sensing* 13 (5): 835–840. doi:10.1080/01431169208904157.

Waske, B., and S. Van Der Linden. 2008. "Classifying Multilevel Imagery from SAR and Optical Sensors by Decision Fusion." *IEEE Transactions on Geoscience and Remote Sensing* 46 (5): 1457–1466. doi:10.1109/TGRS.2008.916089.

Xu, L., J. Li, and A. Brenning. 2014. "A Comparative Study of Different Classification Techniques for Marine Oil Spill Identification Using RADARSAT-1 Imagery." *Remote Sensing of Environment* 141: 14–23. doi:10.1016/j.rse.2013.10.012.

Yamaguchi, Y., T. Moriyama, M. Ishido, and H. Yamada. 2005. "Four-Component Scattering Model for Polarimetric SAR Image Decomposition." *IEEE Transactions on Geoscience and Remote Sensing* 43 (8): 1699–1706. doi:10.1109/TGRS.2005.852084.